DOI 10.1007/s11148-019-00314-0
Refractories and Industrial Ceramics *Vol. 60, No. 1, May, 2019*

MULLITE–TiC–*c*-BN–*c*-ZrO_2 MATERIALS PRODUCED BY SPARK-PLASMA SINTERING AND THEIR PROPERTIES

A. V. Hmelov[1,2]

Translated from *Novye Ogneupory*, No. 2, pp. 23 – 29, February, 2019.

Original article submitted November 20, 2018.

Different *c*-BN/*c*-ZrO_2 ratios are shown to affect the phase composition, microstructure, relative density, open porosity, linear shrinkage, physicomechanical properties, and linear correlation of the elastic modulus and toughness of mullite–TiC–*c*-BN–*c*-ZrO_2 samples during spark-plasma sintering at pressing load 70 MPa and 1200 – 1600°C. The synthesized TiC and *c*-BN powders and *c*-ZrO_2 spark-plasma sintered at 1400°C are characterized by extensive phase crystallization. Mullite and TiC develop profusely in sintered samples with different *c*-BN/*c*-ZrO_2 ratios. Increasing the *c*-BN/*c*-ZrO_2 ratio promotes ingrowth of more *c*-BN than *c*-ZrO_2 at 1200 – 1600°C and causes a less uniformly and densely sintered crystalline microstructure with many pores to form at 1500°C. This sample has lower physicomechanical properties, a poorer linear correlation of elasticity modulus and toughness at 1200 – 1600°C, and lower crack resistance at 1500°C.

Keywords: mullite–TiC–*c*-BN–*c*-ZrO_2 materials, spark-plasma sintering.

The compatibility of oxide and non-oxide powders for spark-plasma sintering deserves special attention [1, 2] because of the different diffusion coefficients in the sintered powders [1 – 3]. It is especially critical for phase transformations, e.g., in boron nitride (BN) as its content in the sintered powder mixture and the temperature increase at low compression loads [1, 4]. This leads to uneven and incomplete sintering of powder mixtures in the transverse and/or longitudinal direction with formation of nonuniformly sintered microstructure and brittleness in boundary areas of oxide and non-oxide crystalline phases. As a result, the crack resistance decreases and the physicochemical properties of the materials are poorer [1 – 4].

The solution to this problem is to add rare-earth metals (e.g., Y_2O_3, Sm_2O_3, Dy_2O_3) that readily form low-melting eutectics with the oxide and non-oxide powders and solid solutions in the liquid phase because of the small cationic radii of the metals in them [5, 6]. The resulting low-melting eutectics promote nucleation of crystalline phases, stimulate diffusion of matter through the eutectic melt, and increase the contact area of the sintered particles. As a result, the powder mixture is more evenly and completely sintered [5 – 7]. The solid solutions compact the structure and strengthen it on microscopic and macroscopic levels at boundary areas of oxide and non-oxide crystalline phases and grain contacts, respectively. As a result, elastic properties are generated, the crack resistance increases, and the physicomechanical properties of the materials improve [7, 8]. On the other hand, these additives oxidize the non-oxide powder, change its composition, and diminish its content. The oxide powder particles have a different effect on sintering of mixtures of oxide and non-oxide powders, grain growth of non-oxide powder, and formation of a different glass-phase composition that increases the brittleness as the additive (oxide component) content, temperature, and compression load increase [8, 9]. As a result, the physicomechanical properties of the materials decrease significantly [8, 9].

ZrO_2 [10] and ZrB_2 powders [11] were added to the mixture of oxide and non-oxide powders to replace the used oxide powder additives and to improve the physicomechanical properties of the materials. However, these components in the powder mixtures caused uneven and incomplete solid-phase sintering. The optimal amount and ratio of additives had to be found to reduce their effects [10, 11].

The goal of the work was to study the effect of different *c*-BN/*c*-ZrO_2 ratios during spark-plasma sintering with compression load 70 MPa at 1200 – 1600°C on the phase composition, microstructure, relative density, open porosity, linear

[1] Institute of Silicate Materials, Riga Technical University, Riga, Latvia.
[2] aleksejs.hmelov44@gmail.com, aleksejs.rtu1@inbox.lv

1083-4877/19/06001-0086 © 2019 Springer Science+Business Media, LLC

shrinkage, physicomechanical properties, and linear correlation of the elasticity modulus and toughness of mullite–TiC–*c*-BN–*c*-ZrO_2 samples.

EXPERIMENTAL

Preparation of mixtures of Al_2O_3 and SiO_2, TiC and *c*-BN powders, and sintered *c*-ZrO_2, preparation of mixtures of oxide and non-oxide powders

Al_2O_3 and SiO_2 powders were mixed (Table 1) according to the published method [12]. TiC and *c*-BN powders were synthesized in a plasma-chemical unit in vacuo at 1600°C for 1 h using TiO_2 (98.0%, Aldrich, Belgium), C (97.5%, Merck, Germany), and B_2O_3 powders (97.5%, Merck, Germany) and N_2 (99.5%, Aldrich, Belgium) and the reactions $TiO_2 + 2C \rightarrow TiC + CO_2$ and $2\ B_2O_3 + 3.5\ N_2 \rightarrow 4\ c\text{-BN} + 3\ NO_2$. Cubic zirconia *c*-$ZrO_2$ was spark-plasma sintered in vacuo at compression load 35 MPa for 2 min at 1400°C. Starting ZrO_2 (97.5%, Merck, Germany) and Y_2O_3 powders (99.5%, Aldrich, Belgium) were used in a 17.58/1 ratio, which corresponded to a biphasic system on the ZrO_2–Y_2O_3 equilibrium phase diagram (by Brown and Odell and Fan Fu-Kanu and Keler) [13]. The component masses (97 mol% ZrO_2/3 mol% Y_2O_3) in units of g per 100 g of mixture were 94.62/5.38.

Samples of powder mixtures of Al_2O_3 and SiO_2, TiC and *c*-BN, and *c*-ZrO_2 were prepared by the published method [12] at compression load 70 MPa.

Method for determining properties of powders and sintered samples

The phase composition of the synthesized and sintered powders, microstructure, relative density ρ_{rel}, open porosity φ, linear shrinkage Δl, elasticity modulus *E*, Vickers hardness *HV*, and surface area *S* of each sample (Table 1) were calculated as before [12]. The theoretical densities (g/cm^3) of the powder components were 3.17, mullite; 4.93, TiC; 3.49, *c*-BN; and 6.27, ZrO_2.

Toughness of the sintered samples was determined by a Vickers microcompression method using an AVK-A Hardness Testing Machine (Akashi Co., Japan) and was calculated using the formula

$$K_{Ic} = 0.073(P/c^{3/2}),$$

where K_{Ic} is the critical strain coefficient or toughness (MPa·m$^{1/2}$); *P*, load applied to test sample surface (kg/cm^2); *c*, half-length of microcracks formed around indenter impression corners (mm).

RESULTS AND DISCUSSION

Figure 1 illustrates the phase compositions of TiC and *c*-BN powders synthesized by a plasma-chemical method. It shows mainly strong diffraction peaks for TiC and *c*-BN with a small amount of TiC_xO_y. This phase was nonstoichiometric TiC containing unreacted TiO_2 and C.

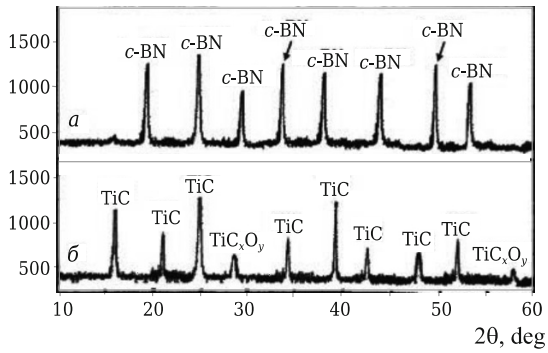

Fig. 1. Phase composition of TiC (*a*) and *c*-BN powders (*b*) synthesized by a plasma-chemical method at 1600°C: TiC_xO_y is titanium oxycarbide.

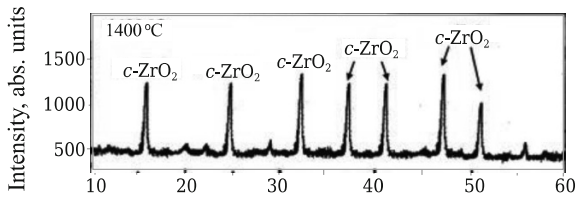

Fig. 2. Phase composition of *c*-ZrO_2 spark-plasma sintered at 1400°C.

Figure 2 illustrates the phase composition of sintered *c*-ZrO_2, which was characterized by distinct diffraction peaks for this phase. This was explained by strain and rearrangement of the ZrO_2 structure from tetragonal to cubic under the compression load and diffusion of Y^{3+} into the *c*-ZrO_2 structure, according to the ZrO_2–Y_2O_3 equilibrium phase diagram (by Brown and Odell and Fan Fu-Kanu and Keler) [13].

Figure 3 shows the phase compositions of mixtures of starting components spark-plasma sintered at 1200 – 1600°C.

Samples of all compositions typically underwent extensive mullitization at 1200 – 1600°C due to structuring and stoichiometric mullite formation. In a similar manner, TiC resulted from a transition into a viscoelastic (plastic) state that promoted diffusion and structuring of TiC under these sintering conditions. Strong ingrowth of *c*-BN and less of *c*-ZrO_2 were observed with increasing *c*-BN/*c*-ZrO_2 ratio at 1200 – 1600°C. However, *c*-BN and *c*-ZrO_2 grew less vigorously than mullite and TiC. This was explained by the denser structures of these components with covalent bonds in *c*-BN. This limited diffusion and structuring of *c*-BN and *c*-ZrO_2 in the solid phase. Also, the ingrowth of *c*-ZrO_2 in the sample with 5 mol% *c*-ZrO_2 was slightly greater than that of *c*-BN in the sample with 5 mol% *c*-BN at 1200 – 1600°C. This was explained by better diffusion into *c*-ZrO_2 than into *c*-BN. In addition, *h*-BN was detectable in the sample with 5 mol% *c*-BN but not in that with 3 mol% *c*-BN because of a partial

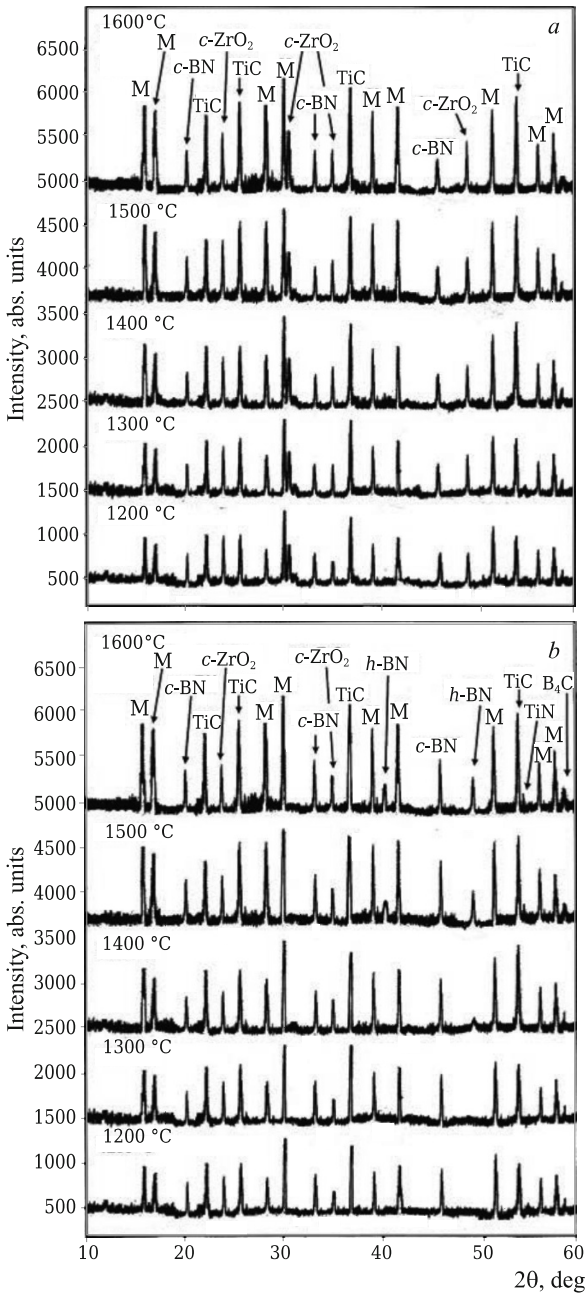

Fig. 3. Phase composition of M92TiC3BN5ZrO_2 (*a*) and M92TiC5BN3ZrO_2 samples (*b*) sintered at 1200 – 1600°C: M, mullite ($3Al_2O_3 \cdot 2SiO_2$); *h*-BN, hexagonal boron nitride; B_4C, boron carbide; TiN, titanium nitride.

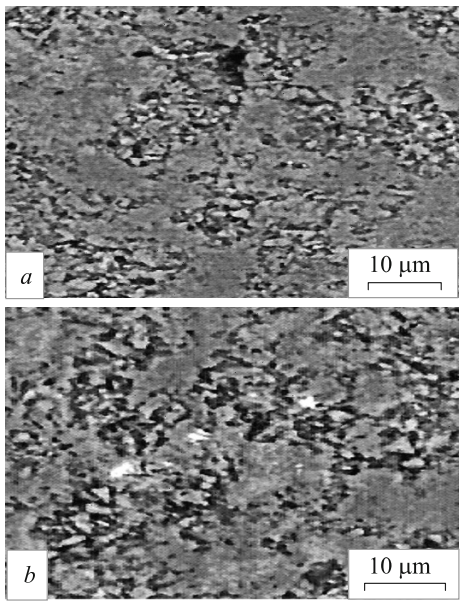

Fig. 4. Microstructure of M92TiC3BN5ZrO_2 (*a*) and M92TiC5BN3ZrO_3 samples (*b*) sintered at 1500°C.

phase transformation of *c*-BN into *h*-BN in the solid in a sintered powder mixture with 5 mol% *c*-BN. These samples had different quantitative ratios of diffraction maxima for *c*-BN and *c*-ZrO_2 at 1200 – 1600°C (Fig. 3) because of different amounts of crystalline phases. The x-ray pattern of the sample with 5 mol% *c*-BN showed weak diffraction peaks for B_4C and TiN that were missing for the sample with 3 mol% *c*-BN at 1500 – 1600°C. These side phases formed from the reaction of TiC and *h*-BN in the sintered powder mixture. Mullite and *c*-ZrO_2 did not react simultaneously with TiC and *c*-BN because decomposition products of mullite and oxidation products of TiC and *c*-BN did not form at 1200 – 1600°C (Fig. 3).

Figure 4 shows microstructures of samples spark-plasma sintered at 1500°C. The microstructure of sintered composition M92TiC3BN5ZrO_2 (Fig. 4*a*) was more uniformly and densely sintered, crystalline, and fine-grained with fewer pores and weakly sintered sections than that of composition M92TiC5BN3ZrO_2 (Fig. 4*b*). This was explained by the different *c*-BN/*c*-ZrO_2 ratios in the sintered compositions (Table 1). Sintering was promoted more by diffusion of the oxide component in the solid phase at high *c*-ZrO_2 and *c*-BN ratios. Viscous flow of mullite and TiC melts also helped to form microstructures with different uniformities and densities. This was explained by the different sintering behaviors of *c*-BN and *c*-ZrO_2 particles in the presence of these melts.

Figures 5 – 8 show measured ρ_{rel}, φ, Δ*l*, *E*, K_{Ic}, *HV*, and a photograph of impressions and microstructures of samples with different *c*-BN/*c*-ZrO_4 ratios at 1200 – 1600°C and 1500°C.

Composition N92TiC3BN5ZrO_2 had a decreased φ and the maximum degree of sintering (91.2%) at 1600°C. This was due to the more even filling of pores because of viscous flow of mullite and TiC melts and initiation of *c*-ZrO_2 diffusion at 1200 – 1300°C. Diffusion of *c*-ZrO_2 became greater than that of *c*-BN in the solid phase at 1300 – 1500°C (Fig. 3*a*). Sintering slowed at 1500 – 1600°C with φ > 8% at 1600°C. This was explained by less extensive and incomplete pore filling during solid-state sintering of *c*-BN and *c*-ZrO_2 particles. The sintering results correlated with the sample microstructure at 1500°C (Fig. 4*a*).

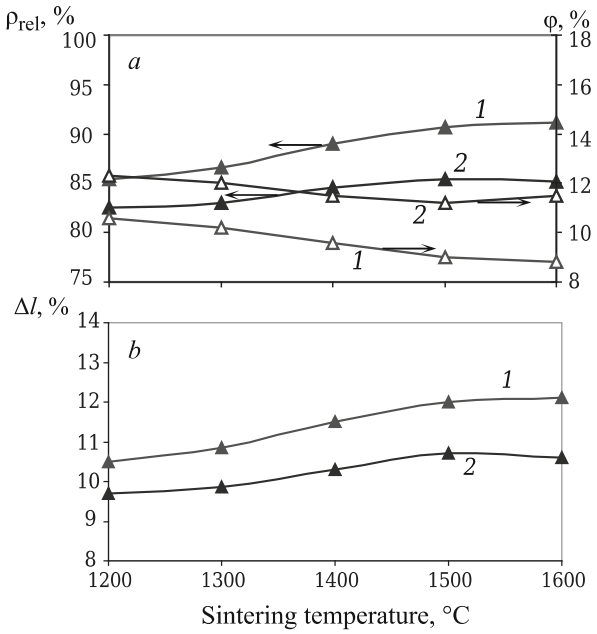

Fig. 5. Parameters ρ_{rel}, φ, and Δl of samples with different *c*-BN/*c*-ZrO_2 ratios that were sintered at 1200 – 1600°C: M92TiC3BN5ZrO_2 (*1*) and M92TiC5BN3ZrO_2 (*2*).

The rises of ρ_{rel} and Δl and fall of φ for composition M92TiC5BN3ZrO_2 at 1200 – 1600°C were irregular. Extensive sintering up to 1400°C was explained by pore filling resulting from viscous flow of mullite and TiC melts (Fig. 3*b*). Slow sintering at 1400 – 1500°C was due to weaker diffusion of *c*-ZrO_2 (at 3 mol%) and *c*-BN because of the increasing partial phase transformation *c*-BN → *h*-BN in the solid phase (Fig. 3*b*) with the latter formed as a layer on the sintered particles that hindered diffusion of matter between particles and pore filling. This was confirmed by studying microstructures of boundary regions of sample crystalline phases (Fig. 6b_1 – b_4). The sintering was reduced somewhat because of the formation of a certain amount of *h*-BN, similar crystalline phases B_4C and TiN (Fig. 3*b*), and a slight porosity increase at 1500 – 1600°C. This correlated with the microstructure of the sample sintered at 1500°C (Fig. 4*b*).

The crystalline, more uniform, and denser sintered fine-grained microstructure of the sample with 3 mol% *c*-BN (Fig. 4*a*) helped significantly to improve the elastic properties and, as a result, to increase the resistance of the sample to external applied loads with high K_{Ic} and *HV* values at 1500°C (Fig. 7). On the other hand, the high parameters for

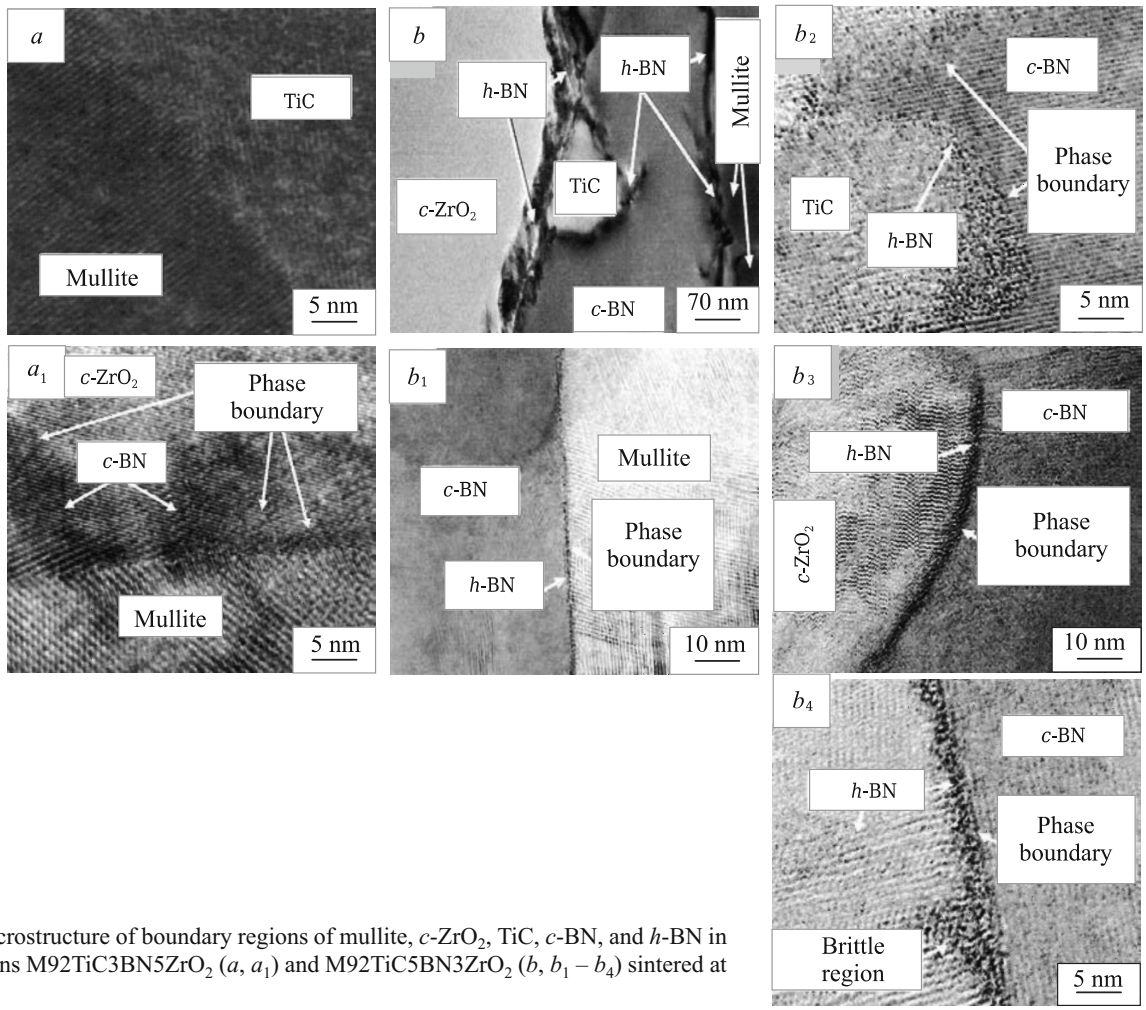

Fig. 6. Microstructure of boundary regions of mullite, *c*-ZrO_2, TiC, *c*-BN, and *h*-BN in compositions M92TiC3BN5ZrO_2 (*a*, a_1) and M92TiC5BN3ZrO_2 (*b*, b_1 – b_4) sintered at 1500°C.

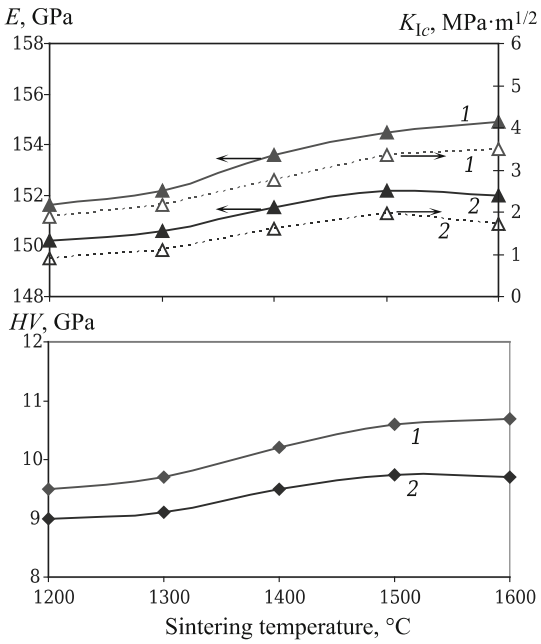

Fig. 7. Parameters E, K_{Ic}, and HV of samples with different c-BN/c-ZrO_2 ratios that were sintered at 1200 – 1600°C: M92TiC3BN5ZrO_2 (*1*) and M92TiC5BN3ZrO_2 (*2*).

these properties were due to insignificant mullite–TiC (Fig. 6*a*), mullite–c-ZrO_2–c-BN, and c-ZrO_2–c-BN boundary regions (Fig. 6a_1). The sample had short microcracks along straight-line trajectories (Fig. 8*a*). The impression showed slight damage as a chip (Fig. 8*a*), indicating little accumulation of internal stresses and minimally brittle boundary regions of these crystalline phases (Fig. 6a, a_1). This corresponded to extensive solid-state sintering of c-ZrO_2 and c-BN particles at 1400 – 1600°C (Fig. 5).

The sample with 5 mol% c-BN had less drastic changes of elastic properties (K_{Ic} and HV) up to 1400°C. The increase of physicomechanical properties slowed at 1400 – 1500°C and decreased slightly at 1500 – 1600°C (Fig. 7). This was due mainly to h-BN formation at boundary sections of sample crystalline phases (Fig. 6b, $b_1 – b_4$) because of partial phase transformation of c-BN into h-BN at 1500 – 1600°C (Fig. 3*b*). The resulting h-BN embrittled the structure with noticeable boundary regions of crystalline phases (Fig. 6*b*) that were less extensive at mullite–c-BN and c-ZrO_2–c-BN boundary regions (Fig. 6b_1, b_3) and more extensive at

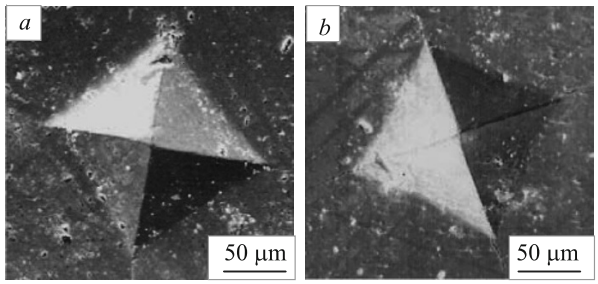

Fig. 8. Impressions from measuring HV on samples M92TiC3BN5ZrO_2 (*a*) and M92TiC5BN3ZrO_2 (*b*) sintered at 1500°C.

TiC–c-BN and c-BN–h-BN boundary regions (Fig. 6$b_1 – b_4$). These properties decreased because the microstructure was incompletely sintered and the sample had many pores (Fig. 4*b*). As a result, the crack resistance of the sample to formation of many microcracks propagating along tortuous trajectories of more weakly sintered regions (Fig. 6b_2, b_4) and chips (Fig. 8*b*) was diminished. This was caused by the high brittleness of the sample at the TiC–c-BN and c-BN–h-BN boundary regions (Fig. 6b_2, b_4).

Figure 9 shows the linear correlation of E and K_{Ic}. A comparison of the R^2 parameters of the approximations with 3 and 5 mol% c-BN showed that the difference was small at 0.01 and was greater for the sample with 3 mol% BN, which agreed with the greater increase of physicomechanical properties (Fig. 7). This was due to the formation of a uniformly and densely sintered fine-grained microstructure with few pores (Fig. 4*a*) and strengthening of the structure at mullite – TiC (Fig. 6*a*), mullite – c-ZrO_2 – c-BN, and c-ZrO_2 – c-BN boundary regions at 1500°C (Fig. 6, a_1). As a result, the E and K_{Ic} values of the sample correlated well with the straight line at 1200 – 1600°C and slightly less at 1400°C. This was related to initiation of solid-state sintering because of extensive diffusion of c-ZrO_2 and less of c-BN at this temperature (Fig. 5). The high correlation of the sample properties with the straight line was indicative of uniform viscous-flow sintering at 1200 – 1300°C and the corresponding solid-state sintering at 1300 – 1600°C.

The lower R^2 values for the sample with 5 mol% c-BN were explained by irregularly and incompletely sintered microstructure with many pores (Fig. 4*b*) and a weaker structure with formation of thicker h-BN in the TiC – c-BN

TABLE 1. Mass Proportions and Component Ratios in Starting Powder Mixtures*

Parameters	Composition	
	M92TiC3BN5ZrO_2	M92TiC5BN3ZrO_2
Mass of TiC/c-BN/c-ZrO_2, g/100 g of mixture	88.94/1.16/9.9	91.85/2.0/6.15
TiC/c-BN/c-ZrO_2 ratio	1.12/86.20/10.1	1.08/50/16.26

* Component mass ($3Al_2O_3/2SiO_2$), g/100 g of mixture, 71.8/28.2.

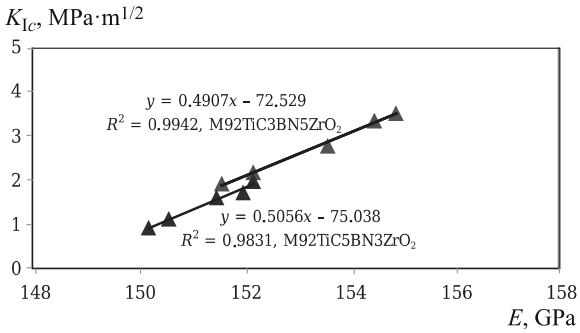

Fig. 9. Linear correlation of E and K_{Ic} for samples sintered at 1200 – 1600°C.

and *c*-BN – *h*-BN boundary regions at 1500°C (Fig. 6, b_2, b_4). As a result, the E and K_{Ic} values deviated more from the straight line at 1600°C than those at 1200, 1300, 1400, and 1500°C, which did not deviate. This indicated that the effects of these processes were greatest and caused nonuniform solid-state sintering of the composition at 1600°C. The different effects of the correlated properties on the R^2 values in both samples were explained by the different sintering mechanisms and, as a result, the different degrees of sintering of the corresponding compositions at 1200 – 1600°C (Fig. 5). The E and K_{Ic} points (values) correlated best with the straight line and, as a result, the R^2 values were greater for the sample with 3 mol% *c*-BN at 1200 – 1600°C because of the complete and uniform solid-phase sintering.

CONCLUSION

Different *c*-BN/*c*-ZrO_2 ratios had different effects during spark-plasma sintering of compositions at compression load 70 MPa and 1200 – 1600°C on the phase composition, microstructure, ρ_{rel}, φ, Δl, physicomechanical properties, and linear correlation of E and K_{Ic} of mullite–TiC–*c*-BN–*c*-ZrO_2 samples. The synthesized TiC and *c*-BN powders and *c*-ZrO_2 spark-plasma sintered at 1400°C were extensively crystallized.

Sintered samples with different *c*-BN/*c*-ZrO_2 ratios showed extensive mullite and TiC ingrowth. Increasing the *c*-BN/*c*-ZrO_2 ratio promoted *c*-BN ingrowth more than *c*-ZrO_2 at 1200 – 1600°C and caused a less uniformly and densely sintered crystalline microstructure with many pores to form at 1500°C. As a result, the sample had lower ρ_{rel}, Δl, and physicomechanical properties at 1200 – 1600°C, less crack resistance at 1500°C, and a poorer linear correlation of E and K_{Ic} at 1200 – 1600°C.

REFERENCES

1. M. Hotta and T. Goto, "Densification and microstructure of Al_2O_3–*c*BN composites prepared spark plasma sintering," *J. Ceram. Soc. Jpn.*, **116**(6), 744 – 748 (2008).
2. S. Chuan, L. Yunkai, W. Yunfei, and Z. Lingbo, "Effect of alumina addition on the densification of boron carbide ceramics prepared by spark plasma sintering technique," *Ceram. Int.*, **40**(8), 12723 – 12728 (2014).
3. A. V. Khmelev, "Preparation of mullite–TiC–ZrC ceramic materials by a plasma-arc method and their properties," *Refract. Ind. Ceram.*, **57**(6), 645 – 650 (2017).
4. P. Klimczyk, M. E. Cura, and A. M. Vlaicu, "Al_2O_3–*c*BN composites sintered by SPS and HPHT methods," *J. Eur. Ceram. Soc.*, **36**(7), 1783 – 1789 (2016).
5. O. Fabrichnaya, G. Savinykh, T. Zienert, and G. Schreiber, "Phase relations in the ZrO_2–Sm_2O_3–Y_2O_3–Al_2O_3 system: Experimental investigation and thermodynamic modelling," *Int. J. Mater. Res.*, **103**(12), 1469 – 1487 (2012).
6. S. Guo and Y. Kagawa, "High-strength zirconium diboride-based ceramic composites consolidated by low temperature hot pressing," *Sci. Technol. Adv. Mater.*, **13**(4), 1 – 6 (2012).
7. X. Zhang, X. Li, J. Han, and W. Han, "Effect of Y_2O_3 on microstructure and mechanical properties of ZrB_2–SiC," *J. Alloys Compd.*, **465**(1/2), 506 – 511 (2008).
8. W. Li, Z. Xinghong, H. Changquing, and H. Jiecai, "Hot-pressed ZrB_2–SiC–YSZ composites with various yttria content: Microstructure and mechanical properties," *Mater. Sci. Eng., A*, **494**(1/2), 147 – 152 (2008).
9. A.-K. Wolfrum, B. Matthey, A. Michaelis, and M. Herrmann, "On the stability of *c*-BN reinforcing particles in ceramic matrix materials," *Materials*, **255**(11), 1 – 17 (2018).
10. D. Chakravarty and G. Sundararajan, "Microstructure, mechanical properties and machining performance of spark plasma sintered Al_2O_3–ZrO_2–TiCN nanocomposites," *J. Eur. Ceram. Soc.*, **33**(13/14), 2597 – 2607 (2013).
11. X. Zhang, W. Li, C. Hong, and W. Han, "Microstructure and mechanical properties of ZrB_2-based composites reinforced and toughened by zirconia," *Int. J. Appl. Ceram. Technol.*, **58**(5), 499 – 504 (2008).
12. A. V. Khmelev, "Preparation of mullite–TiC–TiN materials by plasma spark method and their properties," *Refract. Ind. Ceram.*, **58**(4), 418 – 425 (2017).
13. A. Hmelov, "Synthesis of ceramic powders in the Al_2O_3–SiO_2–ZrO_2 (Y_2O_3) system and production of materials," Doctoral Thesis, Riga Technical University, 2011, pp. 1 – 27.